IOP Publishing | Society for Radiological Protection Journal of Radiological Protection
J. Radiol. Prot. **35** (2015) 777–788 doi:10.1088/0952-4746/35/4/777

A Monte Carlo-based radiation safety assessment for astronauts in an environment with confined magnetic field shielding

Changran Geng[1,2], Xiaobin Tang[1,2], Chunhui Gong[1,2], Fada Guan[3], Jesse Johns[4], Diyun Shu[1,2] and Da Chen[1,2]

[1] Department of Nuclear Science and Engineering, Nanjing University of Aeronautics and Astronautics, Nanjing, People's Republic of China
[2] Collaborative Innovation Center of Radiation Medicine of Jiangsu Higher Education Institutions, Suzhou, People's Republic of China
[3] Department of Radiation Physics, The University of Texas MD Anderson Cancer Center, Houston, TX 77030, USA
[4] Nimbus Innovations, LLC, Temple, TX 76501, USA

E-mail: tangxiaobin@nuaa.edu.cn

Received 17 March 2015, revised 1 August 2015
Accepted for publication 18 August 2015
Published 20 October 2015

Abstract

The active shielding technique has great potential for radiation protection in space exploration because it has the advantage of a significant mass saving compared with the passive shielding technique. This paper demonstrates a Monte Carlo-based approach to evaluating the shielding effectiveness of the active shielding technique using confined magnetic fields (CMFs). The International Commission on Radiological Protection reference anthropomorphic phantom, as well as the toroidal CMF, was modeled using the Monte Carlo toolkit Geant4. The penetrating primary particle fluence, organ-specific dose equivalent, and male effective dose were calculated for particles in galactic cosmic radiation (GCR) and solar particle events (SPEs). Results show that the SPE protons can be easily shielded against, even almost completely deflected, by the toroidal magnetic field. GCR particles can also be more effectively shielded against by increasing the magnetic field strength. Our results also show that the introduction of a structural Al wall in the CMF did not provide additional shielding for GCR; in fact it can weaken the total shielding effect of the CMF. This study demonstrated the feasibility of accurately determining the radiation field inside the environment and evaluating the organ dose equivalents for astronauts under active shielding using the CMF.

Keywords: space radiation, active shielding, confined magnetic field, Geant4, anthropomorphic phantom

(Some figures may appear in colour only in the online journal)

1. Introduction

Two of the crucial problems in space exploration are the risks to astronauts from radiation (Schimmerling *et al* 2003, Durante and Cucinotta 2008, Bahadori *et al* 2011) and to sensitive electronics (McNulty 1996) from ionizing radiation (Reitz 2008). Therefore, an efficient method to protect astronauts from such risks is urgently needed (Schimmerling *et al* 2003, Durante and Cucinotta 2008). Two methods were proposed to shield a spacecraft (Durante and Cucinotta 2011, Durante 2014): passive shielding (Ballarini *et al* 2006) using a bulk material, such as Al, and active shielding (Good 1964, Spillantini 2010, Washburn *et al* 2014), which was proposed in the early 1960s (Good 1964). The fundamental principle of active shielding is to use electromagnetic (EM) fields to deflect incoming charged particles away from a spacecraft, decreasing or avoiding the direct irradiation of the astronauts and devices inside the spacecraft.

Cosmic rays contain a large amount of high-charge and high-energy (HZE) particles, protons, and alpha particles (O'Neill 2010). They contribute significantly to the risk of astronauts experiencing harmful biological effects (Plante and Cucinotta 2008). Galactic cosmic radiation (GCR) distributed in space is a major radiation source, and it is difficult to shield against because of the very high energy of its constituent particles (O'Neill 2010). Theoretically, increasing the thickness of the shielding material of the spacecraft can effectively decrease the harmful effects of the radiation on the astronauts. However, considering the actual payload capacity of a space vehicle, it is not practical to infinitely increase the external shielding. Because of this, the active shielding method may be an effective alternative to the passive shielding method due to its advantage of having a reduced mass (Durante 2014).

To understand the efficiency of the active shielding method in protecting against space radiation, Washburn *et al* (2014) studied the radiation dose reduction at a spatial point using the computer code HZETRN (High charge (Z) and Energy TRaNsport). Papini and Spillantini (2014) estimated the dose reduction through the introduction of the fluence reduction using a toroidal magnetic field.

As the Monte Carlo method is the most accurate way to simulate particle transport, it is expected that it will effectively evaluate the radiation exposure reduction (ICRP 2013) using the active shielding technique. This paper describes a Monte Carlo study that evaluates the reduction of the primary particle fluence, the absorbed dose and the dose equivalent using a confined magnetic field (CMF). The International Commission on Radiological Protection (ICRP) reference anthropomorphic phantom was modeled to mimic an astronaut in a spacecraft. Isotropic particles were modeled as the particle sources in GCR and a solar particle event (SPE). The effects of the structural shielding of a spacecraft were also evaluated for comparison.

2. Materials and methods

2.1. Radiation source

In interplanetary space, two types of radiation, GCR and SPE, always exist. Several GCR fluence models have been built based on the collected data. In this study, the Badhwar–O'Neill

2010 GCR fluence model was used. The model uses a single parameter Φ (in units of MV) for the solar modulation potential to account for the attenuation of the local interstellar spectrum of each element as it travels through the heliosphere (Usoskin *et al* 2005, O'Neill 2010). A larger value of Φ can cause a lower GCR flux. As recommended in the literature (O'Neill 2006), Φ of 450 MV was used to generate the flux spectra of GCR during a solar minimum (figure 1) to simulate the worst case. Detailed information can be found in the study by O'Neill (2010). This analysis only considered particles from 10 MeV n^{-1} to 10^5 MeV n^{-1} for elements with $Z = 1$ through $Z = 28$ because the dose from other elements was negligible (Simpson 1983). In contrast, the SPE event contains protons with a lower energy range and a larger fluence than GCR during an occasional solar flare. One of the classic SPE events, the September 1989 SPE (figure 1) was used in this study because it had the highest intensity in the relativistic range of proton energies since the well-known event of 23 February 1956 (Miroshnichenko *et al* 2000). The considered energy range in SPE (protons only) is from 1 MeV to 1000 MeV. To clarify the shielding efficiency of the CMF, we assumed that the radiation from the top and bottom of the habitat was completely shielded by other components (motors, fuel tanks, etc) of the spaceship following the previous study (Spillantini 2011).

2.2. The Monte Carlo method and physics lists

To determine the dose reduction for astronauts, the Geant4 Monte Carlo toolkit was used in this study (Agostinelli *et al* 2003). Geant4 was originally developed for applications in high-energy, nuclear and accelerator physics. For electromagnetic interaction, Geant4 provides three types of physics list models: Standard, Penelope, and Livermore. For hadronic physics, Geant4 includes diverse physics models, and some reference physics lists which have been designed for different specific applications. For example, the Bertini cascade (BERT) with two basic features (fast and precise) can be used for the Large Hadron Collider (LHC) simulation; however, the binary cascade (BIC) shows better performance for the lower energies of protons and neutrons. The new reference physics list, QBBC, combining the features of BIC in the lower energy range and BERT in the higher energy range, was employed in this study. It has been validated as the most suitable physics list for space applications (Ivantchenko *et al* 2012). The default production cut value of secondary particles of 0.7 mm was used in all simulations. Different types of magnetic fields can also be modeled using Geant4. This study was carried out with Geant4 (version 10.01) on an IBM platform with 14 computation nodes, each of which was configured with an Intel Xeon E5620 2.4 GHz processor and a 24 GB RAM. The number of simulated events was set to 1×10^9 for all cases to make the simulation results meet the relative error of the mean value: $<5\%$.

2.3. Geometry and magnetic field configuration

Two basic candidate configurations of CMF, termed 'toroidal' and 'solenoidal', were proposed by previous investigators (Durante 2014, Papini and Spillantini 2014). However, the rigid toroidal configuration with high-temperature superconductors is believed to be the more realistic possibility in space, and it is largely superior due to the solenoid technology limitations. Hence, we only focused on the toroidal configuration in this study. For the toroidal configuration, the magnetic field distribution is proportional to $1/r$, where r is a variable and represents the radius of the point of interest from the central axis of the habitat. The magnetic field and geometry modeled using Geant4 are illustrated in figure 2. $B0$ represents the intensity of the innermost magnetic field, and $B(r)$ stands for the intensity of the magnetic field at the radius r. R and $R0$ represent the radius of the outermost and innermost limits of the

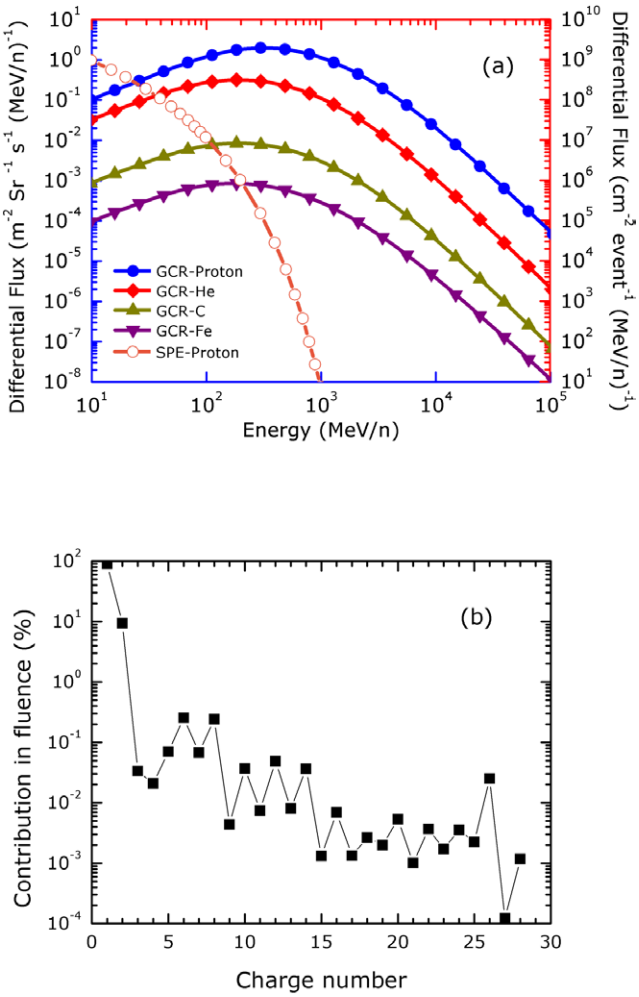

Figure 1. (a) Differential flux spectra of selected GCR particles and SPE protons. The right *Y* axis indicates the scale of the SPE protons, and the left *Y* axis is used for the GCR particles. (b) Relative contribution in fluence of different elements in GCR during a solar minimum.

magnetic field area, respectively, and were set to 5 m and 3 m respectively. As in the previous studies (Durante 2014, Papini and Spillantini 2014), our research also set *B*0 to 2 T, 4 T and 6 T to investigate the active shielding effect. The value 0 T was also studied as a control. The Al layer was set to represent the structural shielding (Ballarini *et al* 2006). Different Al thicknesses ranging from 10 to 50 g cm^{-2} with an increment of 10 g cm^{-2} were modeled to investigate the effects of the structural shielding.

2.4. Dose estimation

Absorbed dose (D) is a physical quantity that is defined as the mean energy imparted to matter per unit mass by ionizing radiation. Specifically, absorbed dose to a tissue or organ (D_T) is

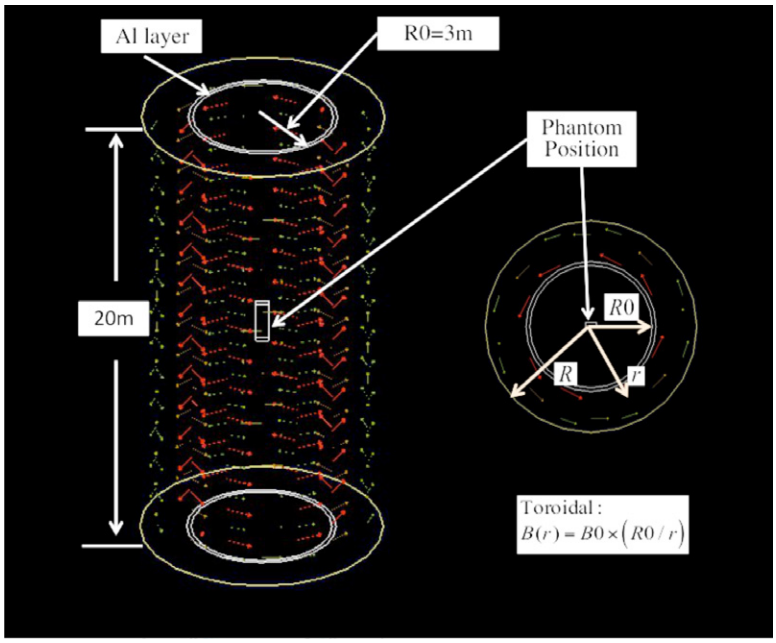

Figure 2. Configuration of toroidal fields in Geant4 rendered by an OpenGL visualization driver. The arrows represent the orientation of the magnetic field, and different colors represent different magnetic field intensities (red: higher, green: lower).

the quotient of the deposited energy and the tissue or organ mass. According to the National Council on Radiation Protection & Measurements (NCRP) Report No. 132 (2000) and ICRP Report No. 123 (2013), to quantify the biological effects of different types of radiation, the unrestricted linear energy transfer (LET)-based quality factor (Q (LET)), rather than the radiation weighting factor (Pelliccioni 1998), was used to calculate the organ specific dose equivalent, H_T. The process to calculate H_T followed the procedure described in ICRP Report No. 123 (2013). In Geant4, the LET can be calculated by dividing the energy deposition by the tracking step length of each specified type of charged particles. The LET-based quality factor was calculated as follows (ICRP 1991)

$$Q(\mathrm{LET}) = \begin{cases} 1, \ \mathrm{LET} < 10\ \mathrm{keV}\ \mu\mathrm{m}^{-1} \\ 0.32 \times \mathrm{LET} - 2.2, \ 10 \leqslant \mathrm{LET} \leqslant 100\ \mathrm{keV}\ \mu\mathrm{m}^{-1} \\ 300/\sqrt{\mathrm{LET}}, \ \mathrm{LET} > 100\ \mathrm{keV}\ \mu\mathrm{m}^{-1} \end{cases} \quad (1)$$

The 'male effective dose', which summed up the organ dose equivalent with the tissue weighting factors recommended in ICRP, was calculated to serve as a useful indicator of overall dosimetric characteristics (Lee 2006, Cassola *et al* 2010). The combination of a computational phantom and the Monte Carlo method is a feasible approach to calculate the organ doses in complex radiation fields (Maynard *et al* 2011, Geng *et al* 2014). The ICRP reference male phantom was used in this study, which was published in 2009 as the recommended phantom for radiation studies. The phantom was based on medical imaging data, consistent with the reference for anatomical and physiological parameters given in the ICRP Report No. 89 (2002). To estimate radiation dose to the representative astronaut with the shielding of the CMF, the human phantom was located at the center of the habitat, illustrated in figure 2.

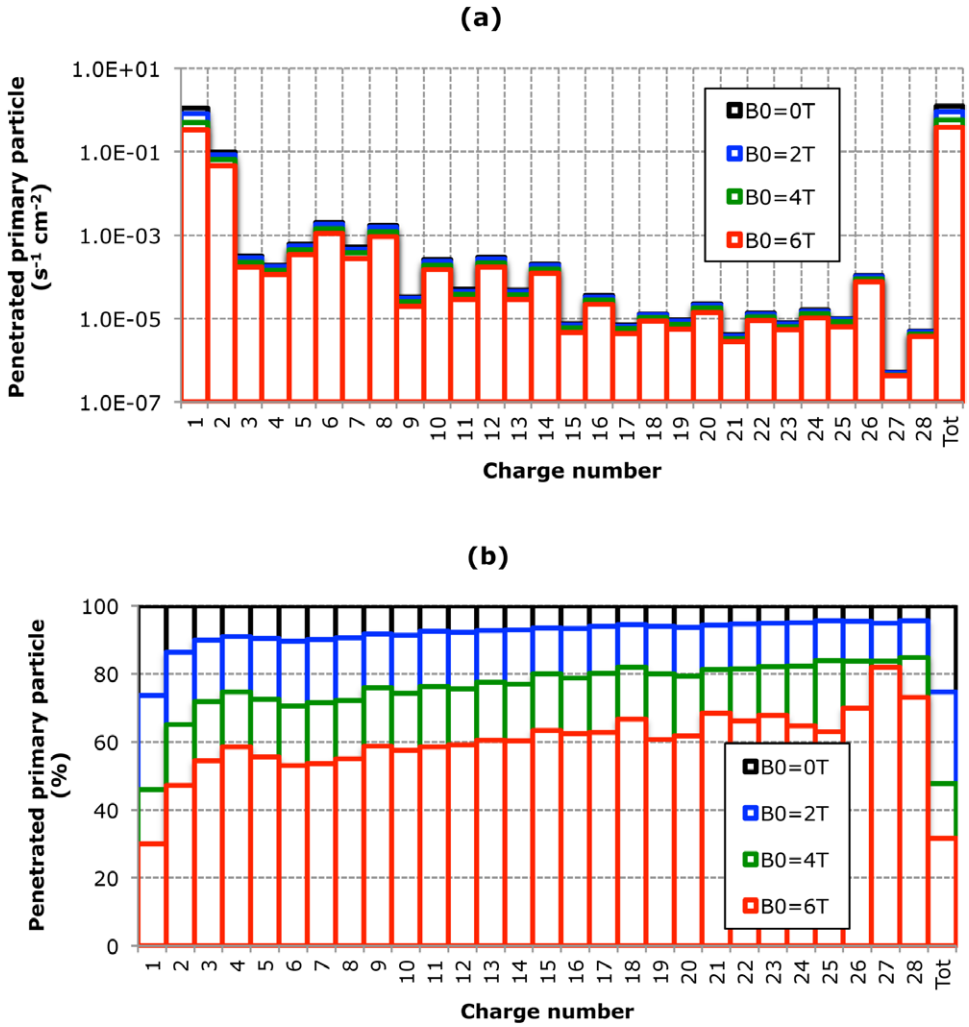

Figure 3. Number of the penetrated primary GCR particles (from $Z = 1$ to 28, and total) through a toroidal field and the 10 g cm^{-2} Al equivalent shielding. (a) The absolute value is normalized by the area of the inner surface of the cylindrical habitat per second. (b) The relative value (%) is normalized by the result with $B0 = 0$ T. The standard error is $<5\%$ for all data points.

3. Results and discussion

3.1. Reduction of the fluence by the toroidal field

First, we studied the penetrating fluence of primary particles through toroidal fields with a 10 g cm^{-2} structural Al equivalent shielding. This represents the structural/passive shielding of the spaceship wall structure. The shielding ability of the toroidal field is determined by the bending power (the magnetic field strength multiplied by the field thickness, BL) (Durante 2014), where B is the field flux density and L is the particle field thickness. In principle, BL can be calculated by $\int_{R0}^{R}(B0 \times R0/r)\,\mathrm{d}r$ for the toroidal field. According to the settings illustrated in figure 2, when $B0$ is 6 T, the calculated BL is equal to 9.19 Tm in this field.

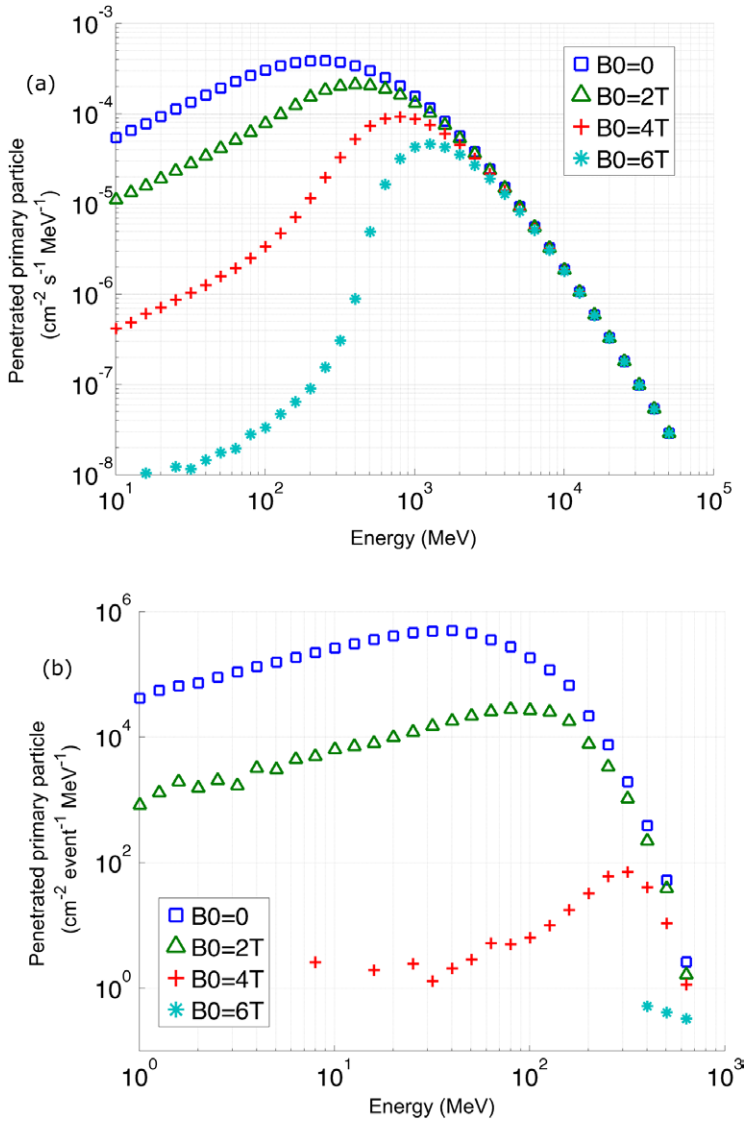

Figure 4. Differential flux spectra of the penetrated primary (a) GCR protons and (b) SPE protons through a toroidal field with 10 g cm^{-2} Al equivalent structure shielding.

As expected, for both GCR and SPE protons the penetrating primary particles decreased with the increase of $B0$(see figure 3). Panel (a) shows the absolute values plotted in a log scale to clearly present the wide magnitude of the results for different particles. However, this plot may not make clear the impact of different magnetic field strengths for each particle. Hence, in panel (b), the relative values from different magnetic field strengths normalized by the result with $B0 = 0$ T are provided. With the increase of the charge number, the reduction rate of flux decreases. The total number of penetrating primary particle decreases from 1.22 s^{-1} cm^{-1} to 0.38 s^{-1} cm^{-1} when $B0$ increases from 0 T to 6 T. For SPE, the percentages of the penetrating primary particles are 55.57%, 9.74%, and 0.000 3% for $B0 = 2$ T, 4 T and 6 T relative to $B0 = 0$ T, respectively. The reduction rate per $B0$ for SPE was much higher than that for GCR

Table 1. Organ dose equivalent (Sv/event) and male effective dose (Sv/event) in the ICRP reference male phantom resulted by SPE protons with the toroidal field with 10 g cm^{-2} Al equivalent structure shielding. The percentage of dose values from different magnetic field strengths relative to the result from $B0 = 0$ T are also listed.

	Organ dose equivalent or male effective dose (Sv/event)				Percentage of dose values to the result from $B0 = 0$ T		
$B0$ (T)	0	2	4	6	2	4	6
Skin	8.39E − 01	8.60E − 02	1.84E − 04	7.21E − 05	10.3%	0.0%	0.0%
Liver	2.00E − 01	4.61E − 02	2.84E − 04	1.25E − 06	23.1%	0.1%	0.0%
Brain	4.81E − 01	7.14E − 02	1.01E − 04	4.70E − 05	14.8%	0.0%	0.0%
Heart	1.49E − 01	4.81E − 02	4.84E − 04	2.82E − 04	32.3%	0.3%	0.2%
Muscle	4.92E − 01	7.00E − 02	4.62E − 04	1.00E − 04	14.2%	0.1%	0.0%
Effective	2.62E − 01	6.20E − 02	2.93E − 04	5.89E − 05	23.7%	0.1%	0.0%

Table 2. Male effective dose (Sv/s) by GCR particles (from $Z = 1$ to 28, and total) with the toroidal field in the ICRP reference male phantom with a 10 g cm^{-2} structural Al equivalent shielding. The percentage of dose values from different magnetic field strengths relative to the result from $B0 = 0$ T are also listed.

	Male effective dose (Sv s^{-1})				Percentage of dose values to the result from $B0 = 0$ T		
$B0(T)$	0	2	4	6	2	4	6
$Z = 1$	7.66E − 09	7.60E − 09	6.60E − 09	5.77E − 09	99.2%	86.2%	75.3%
$Z = 2$	2.47E − 09	2.45E − 09	2.31E − 09	2.08E − 09	99.2%	93.5%	84.2%
$Z = 8$	1.27E − 09	9.82E − 10	8.22E − 10	5.70E − 10	77.3%	64.7%	44.9%
$Z = 26$	2.53E − 09	2.05E − 09	1.86E − 09	1.29E − 09	81.0%	73.5%	51.0%
Others	4.40E − 09	4.29E − 09	3.96E − 09	3.13E − 09	97.5%	90.0%	71.1%
Total	1.83E − 08	1.74E − 08	1.55E − 08	1.28E − 08	95.1%	84.7%	69.9%

because the energy range of SPE is relatively lower than that of GCR, as shown in figure 1. Figures 4(a) and (b) show the differential flux spectra of primary protons penetrating into the habitat from GCR and SPE, respectively. For $B0 = 4$ T and 6 T, there are rare SPE protons with energy lower than 20 MeV and 500 MeV penetrating into the habitat with the combination of the structural Al shielding and the toroidal field; as a result, no data points lower than these threshold energies in the corresponding spectra are shown in figure 4(b). For GCR, we can still see the much lower energy components in the spectra for $B0 = 4$ T and 6 T. The differences between figures 4(a) and (b) can be attributed to energy range differences and the shape of the initial source particle energy spectra shown in figure 1, where SPE has a much lower energy range and a much higher proportion of low energy protons.

3.2. Dose reduction by CMF

One can expect that the dose and dose equivalent from space radiation should be decreased with the increased $B0$ since the primary particles can be deflected by the toroidal field without

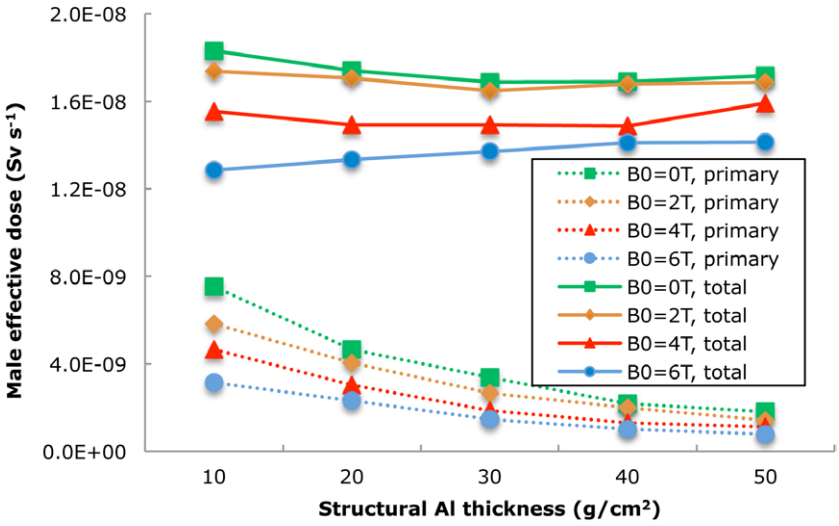

Figure 5. The variation of male effective dose with the increased structural Al thickness. The standard error is <5% for all data points. 'Primary' refers to the dose results from primary particles only; 'total' means the dose results from all types of particles including primary and secondary particles.

the production of secondary particles. However, the existence of structural shielding produced unexpected results because of the production of secondary particles in the shielding material.

The organ dose equivalent and male effective dose for the SPE protons are listed in table 1. The results clearly show that the shielding effect of the toroidal field increases with $B0$. When $B0$ was 6 T for the toroidal field, the skin dose was reduced from 0.839 Sv/event ($B0 = 0$ T) to 7.21×10^{-5} Sv/event. The dose to internal organs, such as the liver, was lower than that to the skin. The male effective dose decreased from 0.262 Sv/event to 5.89×10^{-5} Sv/event as $B0$ increased from 0 T to 6 T.

The male effective dose from GCR particles with the shielding of toroidal field and a 10 g cm^{-2} Al structural shielding are listed in table 2. The results show that the male effective dose reduces from 1.83×10^{-8} to 1.28×10^{-8} Sv s^{-1} as $B0$ increases from 0 T to 6 T. For each particle type (same Z) in GCR, the male effective dose decreased with the increase of $B0$. This variation is similar to the reduction of the penetrating primary particles. This tendency is also in line with the previous study using the HZETRN code (Washburn *et al* 2014).

3.3. Effects from passive/structural shielding

We also investigated the effects of different thicknesses of the passive/structural shielding on the dose reduction combined with the toroidal magnetic field in the GCR environment. Figure 5 shows the male effective dose of primary particles as well as of both primary and secondary particles ('total'), with different structural Al thickness for every considered magnetic field. Our results clearly show that with each fixed structural thickness, the higher magnetic field intensity will always have the stronger shielding effect. As expected, the effective dose from the primary particles decreases exponentially with increasing Al thickness for every $B0$. However, the total male effective dose did not always decrease with the increase of the Al thickness. For $B0 = 0$ T and 2 T, the male effective dose decreases by 8% with the structural Al thickness from 10 g cm^{-2} to 30 g cm^{-2}, and it appears that greater thickness has no shielding

effect. For $B0 = 4$ T, the male effective dose is reduced only by 4% when the structural Al thickness is increased from 10 g cm^{-2} to 20 g cm^{-2}; greater Al thickness has no additional shielding effect, and may even weaken the total shielding effect. For $B0 = 6$ T, the dose was increased slightly with increased structural Al thickness, which also showed that the thicker wall structure can have a negative effect on the total radiation shielding. This can be attributed to the balance of the dose contributions from the primary particles and the secondary particles generated in the structural wall. Although the thicker structure can effectively decrease the fluence of the primary particles, it can on the other hand also increase the production of secondary particles, which can also contribute to the dose to the human body inside the habitat. In the study by Washburn *et al* (2014), the dose results were calculated at a spatial point neglecting the interactions of radiation with the human body using the deterministic radiation code HZETRN. Therefore, the differences between our results using the Monte Carlo method and their deterministic results are understandable (Heinbockel *et al* 2011a, 2011b).

4. Conclusion

Our approach first demonstrated the feasibility of the Monte Carlo simulation in investigating the radiation safety problems inside an environment under CMF shielding. The ICRP reference voxel phantom was incorporated to calculate the organ dose and dose equivalent. The calculated particle fluence, dose equivalent and male effective dose in the ICRP male phantom with GCR and SPE radiation showed that the higher magnetic field can provide more effective protection to the astronauts in the spacecraft. However, due to the larger energy range and multiple particle species, the shielding for GCR is more complex, especially considering the effect of the additional but unavoidable structural wall of the spacecraft. With higher magnetic fields in active shielding, the total effectiveness is weakened by using thicker Al structural shielding. This can be attributed to the increased production of secondary particles in the structural material of the spacecraft. Therefore, other structural shielding materials with a lower production rate of secondary particles, such as hydrocarbons (Cucinotta *et al* 2012) might serve as a better alternative.

Although we demonstrated the effectiveness of the active shielding, this study has some limitations because we did not apply it to a realistic situation. First, the radiation from the top and bottom of the habitat was not simulated. Second, detailed information about the habitat and the aircraft was lacking. Further studies are already under way to simulate more realistic situations on the International Space Station and Mars using the method developed in this study, which can also be extended to other applications such as evaluating the radiation effects with more complicated magnetic fields. One can expect that, regarding specific magnetic field configurations in further designs (such as the 'DOUBLE HELIX' toroidal field developed in the active radiation shield for space exploration missions (ARSSEM)) , ANASYS or COMSOL software may be used to generate the magnetic field to be imported into the Geant4 Monte Carlo code.

Acknowledgments

This work was partially funded by National Natural Science Foundation of China (No. 11475087), the funding of Jiangsu Innovation Program for Graduate Education (No. KYLX_0265), the Fundamental Research Funds for the Central Universities (No. NS2014060), and a project funded by the Priority Academic Program Development of Jiangsu Higher Education Institutions.

References

Agostinelli S, Allison J, Amako K A, Apostolakis J, Araujo H, Arce P, Asai M, Axen D, Banerjee S and Barrand G 2003 GEANT4—a simulation toolkit *Nucl. Instrum. Methods Phys. Res.* A **506** 250–303

Bahadori A A, Van Baalen M, Shavers M R, Dodge C, Semones E J and Bolch W E 2011 The effect of anatomical modeling on space radiation dose estimates: a comparison of doses for NASA phantoms and the 5th, 50th, and 95th percentile male and female astronauts *Phys. Med. Biol.* **56** 1671

Ballarini F, Battistoni G, Cerutti F, Fasso A, Ferrari A, Gadioli E, Garzelli M, Mairani A, Ottolenghi A and Paretzke H 2006 GCR and SPE organ doses in deep space with different shielding: Monte Carlo simulations based on the FLUKA code coupled to anthropomorphic phantoms *Adv. Space Res.* **37** 1791–7

Cassola V F, Kramer R, Brayner C and Khoury H J 2010 Posture-specific phantoms representing female and male adults in Monte Carlo-based simulations for radiological protection *Phys. Med. Biol.* **55** 4399–430

Cucinotta F A, Kim M-H Y and Chappell L J 2012 Evaluating shielding approaches to reduce space radiation cancer risks *NASA Technical Memorandum* 217361

Durante M 2014 Space radiation protection: destination Mars *Life Sci. Space Res.* **1** 2–9

Durante M and Cucinotta F A 2008 Heavy ion carcinogenesis and human space exploration *Nat. Rev. Cancer* **8** 465–72

Durante M and Cucinotta F A 2011 Physical basis of radiation protection in space travel *Rev. Mod. Phys.* **83** 1245–81

Geng C, Tang X, Hou X, Shu D and Chen D 2014 Development of Chinese hybrid radiation adult phantoms and their application to external dosimetry *Sci. China Technol. Sci.* **57** 713–9

Good R C, Shen S P and Dow N F 1964 Active shielding concepts for the ionizing radiation in space *Report Numbers* N64-31552; NASA-CR-58950

Heinbockel J H *et al* 2011a Comparison of the transport codes HZETRN, HETC and FLUKA for a solar particle event *Adv. Space Res.* **47** 1079–88

Heinbockel J H *et al* 2011b Comparison of the transport codes HZETRN, HETC and FLUKA for galactic cosmic rays *Adv. Space Res.* **47** 1089–105

ICRP 1991 1990 Recommendations of the International Commission on Radiological Protection, ICRP Publication 60 *Ann. ICRP 21*

ICRP 2002 Basic anatomical and physiological data for use in radiological protection reference values, ICRP Publication 89 *Ann. ICRP 32*

ICRP 2009 Adult reference computational phantoms, ICRP Publication 110 *Ann. ICRP 39*

ICRP 2013 Assessment of radiation exposure of astronauts in space, ICRP Publication 123 *Ann. ICRP 42*

Ivantchenko A V, Ivanchenko V N, Molina J-M Q and Incerti S L 2012 Geant4 hadronic physics for space radiation environment *Int. J. Radiat. Biol.* **88** 171–5

Lee C 2006 Development of the voxel computational phantoms of pediatric patients and their application to organ dose assessment *Nuclear and Radiological Engineering* (Gainesville, FL: University of Florida)

Maynard M R, Geyer J W, Aris J P, Shifrin R Y and Bolch W 2011 The UF family of hybrid phantoms of the developing human fetus for computational radiation dosimetry *Phys. Med. Biol.* **56** 4839

McNulty P J 1996 Single-event effects experienced by astronauts and microelectronic circuits flown in space *IEEE Trans. Nucl. Sci.* **43** 475–82

Miroshnichenko L I, De Koning C A and Perez-Enriquez R 2000 Large solar event of September 29, 1989: ten years after *Space Sci. Rev.* **91** 615–715

NCRP 2000 Radiation protection guidance for activities in low-earth orbit *NCRP Report* 132

O'Neill P M 2006 Badhwar–O'Neill galactic cosmic ray model update based on advanced composition explorer (ACE) energy spectra from 1997 to present *Adv. Space Res.* **37** 1727–33

O'Neill P M 2010 Badhwar–O'Neill 2010 galactic cosmic ray flux model—revised *IEEE Trans. Nucl. Sci.* **57** 3148–50

Papini P and Spillantini P 2014 Toroidal magnetic fields for protecting astronauts from ionizing radiation in long duration deep space missions *Acta Astronaut.* **104** 531–7

Pelliccioni M 1998 Radiation weighting factors and high energy radiation *Radiat. Prot. Dosim.* **80** 371–8

Plante I and Cucinotta F A 2008 Ionization and excitation cross sections for the interaction of HZE particles in liquid water and application to Monte Carlo simulation of radiation tracks *N. J. Phys.* **10** 125020

Reitz G 2008 Characteristic of the radiation field in low Earth orbit and in deep space *Z. Med. Phys.* **18** 233–43

Schimmerling W, Cucinotta F A and Wilson J W 2003 Radiation risk and human space exploration *Adv. Space Res.* **31** 27–34

Simpson J A 1983 Elemental and isotopic composition of the galactic cosmic rays *Annu. Rev. Nucl. Part. Sci.* **33** 323–82

Spillantini P 2010 Active shielding for long duration interplanetary manned missions *Adv. Space Res.* **45** 900–16

Spillantini P 2011 Superconducting magnets and mission strategies for protection from ionizing radiation in interplanetary manned missions and interplanetary habitats *Acta Astronaut.* **68** 1430–9

Usoskin I G, Alanko-Huotari K, Kovaltsov G A and Mursula K 2005 Heliospheric modulation of cosmic rays: monthly reconstruction for 1951–2004 *J. Geophys. Res.* **110** A12108

Washburn S A, Blattnig S R, Singleterry R C and Westover S C 2014 Analytical-HZETRN model for rapid assessment of active magnetic radiation shielding *Adv. Space Res.* **53** 8–17